# TOWARDS AN EMPIRICAL DETERMINATION OF THE ZZ CETI INSTABILITY STRIP

A. Gianninas, P. Bergeron, and G. Fontaine

Département de Physique, Université de Montréal, C.P. 6128, Succ. Centre-Ville, Montréal, Québec, Canada, H3C 3J7.

## ABSTRACT

We present atmospheric parameters for a large sample of DA white dwarfs that are known to be photometrically constant. For each star, we determine the effective temperature and surface gravity by comparing high signal-to-noise ratio optical spectra to the predictions of detailed model atmosphere calculations. We also report the successful prediction and detection of photometric variability in G232-38 based on similar  $T_{\text{eff}}$  and  $\log g$  determinations. The atmospheric parameters derived for this sample of constant stars as well as those for the known sample of bright ZZ Ceti stars (now boosted to a total of 39) have been obtained in a highly homogeneous way. We combine them to study the empirical red and blue edges as well as the purity of the ZZ Ceti instability strip. We find that the red edge is rather well constrained whereas there exists a rather large range of possibilities for the slope of the blue edge. Furthermore, the ZZ Ceti instability strip that results from our analysis contains no nonvariable white dwarfs. Our sample of constant stars is part of a much broader spectroscopic survey of bright (V < 17) DA white dwarfs, which we have recently undertaken. We also present here some preliminary results of this survey. Finally, we revisit the analysis by Mukadam et al. of the variable and nonvariable DA stars uncovered as part of the Sloan Digital Sky Survey. Their erroneous conclusion of an instability strip containing several nonvariable stars is traced back to the low signal-to-noise ratio spectroscopic observations used in that survey.

Subject headings: stars: individual (G232-38) - stars: oscillations - white dwarfs

# 1. INTRODUCTION

The ZZ Ceti stars represent a class of variable white dwarfs whose optical spectra are dominated by hydrogen lines (DA stars). They occupy a narrow region in the  $T_{\rm eff}$ -log g plane known as the ZZ Ceti instability strip, with an average effective temperature around  $T_{\rm eff} \sim 11,600~{
m K}$  and a width of roughly 1000 K. A precise determination of the hot and cool boundaries of this instability strip may eventually provide important constraints about the structure of the outer layers of DA white dwarfs. For instance, it has been originally shown by Winget et al. (1982) that the location of the blue edge is sensitive to the convective efficiency in the hydrogen zone, which led Fontaine, Tassoul, & Wesemael (1984) to propose using this property as a potential calibrator of the mixing-length theory in pulsating white dwarfs. Similarly, the location of the red edge may help us understand the mechanism responsible for the disappearance of the ZZ Ceti phenomenon at low temperatures, which seems to be related to either convective mixing of the hydrogen outer layer with the deep helium envelope or the interaction of pulsation with convection (Tassoul et al. 1990). Also of utmost importance is to determine whether all white dwarfs within the ZZ Ceti instability strip are pulsators. If the strip is indeed pure, as first suggested by Fontaine et al. (1982), ZZ Ceti stars would necessarily represent a phase through which all DA stars must evolve, and thus the results from asteroseismological studies might provide constraints on the properties not only of known ZZ Ceti stars, but on the whole population of DA stars as well.

Determinations of the boundaries of the ZZ Ceti instability strip prior to 1991 have been nicely summarized by Wesemael et al. (1991) who discuss the results from various observational techniques, both photometric and spectroscopic. Among the first photometric studies were those conducted using Strömgren photometry by McGraw (1979) and later by Fontaine et al. (1985). Both analyses made it evident that ZZ Ceti stars formed a rather homogeneous class of DA white dwarfs in color-color diagrams, a result that was not obvious from prior analyses based on broad-band colors. Multichannel spectrophotometric data of ZZ Ceti stars obtained by Greenstein (1976) have been analyzed by Fontaine et al. (1982), Greenstein (1982), and by Weidemann & Koester (1984) using slightly different absolute flux calibrations.

Later on, Wesemael et al. (1986), Lamontagne et al. (1987), and Lamontagne et al. (1989) have used ultraviolet spectra obtained by the IUE satellite as an independent method of measuring the effective temperature of ZZ Ceti stars. In their analysis they assumed a value of  $\log g = 8$  for each star but also mentioned that this assumption could be a source of uncertainty as several ZZ Ceti stars showed signs of having  $\log g$  significantly higher or lower (e.g., G226-29 and Ross 548, respectively). Finally, Daou et al. (1990) have carried out the first analysis of a set of ZZ Ceti stars using the spectroscopic technique where optical

spectroscopic observations of the individual Balmer lines are fitted with synthetic spectra to obtain measures of both  $T_{\text{eff}}$  and  $\log g$ .

The effective temperatures for the ZZ Ceti stars inferred from these photometric and spectroscopic studies are in fairly good agreement according to Figure 1 of Wesemael et al. (1991), with the blue edge in the range  $T_{\rm eff} = 12, 130-13, 500$  K and the red edge in the range  $T_{\rm eff} = 10,000-11,740$  K. However, this apparent agreement has been seriously questioned by Bergeron et al. (1992b) who examined the effects of different convective efficiencies on the optical spectra of DA white dwarfs in the vicinity of the ZZ Ceti instability strip. The results of their calculations showed that the predicted absolute fluxes, color indices, and equivalent widths are sensitive to the convective efficiency in the range  $T_{\rm eff} \sim 8000-15,000$  K, with a maximum sensitivity around 13,000 K. Hence, without a detailed knowledge of the convective efficiency in the atmosphere of ZZ Ceti stars, the results from all previous photometric and spectroscopic analyses had to be considered uncertain.

This problem of the convective efficiency in the atmosphere of ZZ Ceti stars has been tackled by Bergeron et al. (1995c, B95 hereafter) who used optical spectroscopic observations combined with UV energy distributions to show that the so-called  $ML2/\alpha = 0.6$  parametrization of the mixing-length theory provides the best internal consistency between optical and UV effective temperatures, trigonometric parallaxes, V magnitudes, and gravitational redshifts. With the atmospheric convective efficiency properly parameterized, the spectroscopic technique could now yield atmospheric parameters  $T_{\text{eff}}$  and  $\log g$  for the ZZ Ceti stars that were not only accurate in a relative sense, but in an absolute sense as well. Hence it was possible for the first time to demonstrate that the boundaries of the ZZ Ceti instability strip were a function of both the effective temperature and the surface gravity of the star. Our knowledge of the boundaries of the ZZ Ceti instability strip prior to the study of Mukadam et al. (2004b) discussed below is summarized in Figure 4 of Bergeron et al. (2004). The ZZ Ceti stars occupy a trapezoidal region in the  $T_{\text{eff}} - \log g$  plane, with the blue edge showing a stronger dependence on the surface gravity than the red edge does. Consequently the width of the instability strip is also gravity-dependent, with  $\Delta T_{\rm eff} \sim 800$  K at  $\log g = 7.5$  and nearly twice as wide at  $\log g = 8.5$ .

As mentioned above, the assessment of the purity of the instability strip is also of considerable interest. More than twenty years ago, Fontaine et al. (1982) have argued from their study of multichannel spectrophotometric data that the strip is most likely pure, and that ZZ Ceti stars therefore represent an evolutionary phase through which all DA white dwarfs must pass. This conclusion is strongly supported by our spectroscopic analysis of the 36 known ZZ Ceti stars shown in Figure 4 of Bergeron et al. (2004). The latter also included 54 known nonvariable white dwarfs that were all found to lie clearly outside the empirical

instability strip. We note that, prior to this effort, the purity of the instability strip had been questioned repeatedly (Dolez et al. 1991; Kepler & Nelan 1993; Kepler et al. 1995; Silvotti et al. 1997; Giovannini et al. 1998).

More recently, Mukadam et al. (2004a) reported the discovery of 35 new ZZ Ceti stars from the Sloan Digital Sky Survey (SDSS) along with a large number of stars found to be photometrically constant. Mukadam et al. (2004b) used the results from this sample of both variable and nonvariable DA stars to "redefine" the location of the instability strip and to assess its purity. Although their determinations of  $T_{\rm eff}$  and  $\log g$  for these new ZZ Ceti stars place virtually all of the variables within the instability strip defined by Bergeron et al. (2004), with a possible offset due to the use of a different set of model spectra (see § 3), they also found a large fraction of nonvariable stars within the strip. These results are clearly at odds with the conclusions from our work during the last ten years.

In this respect, we have been gathering over the recent years optical spectroscopic observations for all known nonvariable DA white dwarfs with the goal of (1) constraining the location of the boundaries of the ZZ Ceti instability strip not only by analyzing the variable stars within the strip itself, but also the photometrically constant stars in its vicinity, and (2) increasing the statistical significance of the purity of the empirical instability strip. Some partial results from this endeavor have been reported in Bergeron et al. (2004). Here we present the results of our entire sample in § 2, which include the discovery of a new ZZ Ceti star. In § 3 we revisit the results of Mukadam et al. (2004b) for the variable and nonvariable DA stars uncovered in the SDSS. We then report in § 4 on preliminary results of a much broader spectroscopy survey of the white dwarf catalog of McCook & Sion (1999). Our conclusions follow in § 5.

## 2. PHOTOMETRIC SAMPLE

# 2.1. Spectroscopic Observations

Our sample of photometrically constant DA stars is composed of 121 objects gathered from various sources. Firstly, we have searched the literature for all mentions of DA white dwarfs observed in high-speed photometry and where no variations were detected. These include two Ph.D. theses (McGraw 1977; Giovannini 1996) and several studies of the instability strip including those of Dolez et al. (1991), Kepler et al. (1995), and Giovannini et al. (1998). Another source consists of previously unpublished data from various observing campaigns conducted over the years by two of us (GF and PB) and collaborators. We were also able to include 4 white dwarfs identified in the Hamburg Quasar Survey and reported

to be constant by Mukadam et al. (2004a). Our sample does not include, however, stars whose nonvariability has recently come to our attention such as those reported by Silvotti et al. (2005) nor those discovered in the SDSS by Mukadam et al. (2004a) and Mullally et al. (2005).

Our sample of 121 nonvariable DA stars is listed in Table 1 in order of increasing right ascension. About 30% of the spectra in this sample were already available from the previous spectroscopic analyses of Bergeron et al. (1992a) and Bergeron et al. (1995a). These spectra had been secured using our standard setup at the Steward Observatory 2.3 m telescope equipped with the Boller & Chivens spectrograph. The 4."5 slit together with the 600 line mm<sup>-1</sup> grating blazed at 3568 Å in first order provides a spectral coverage from about 3000 to 5250 Å at a resolution of  $\sim$  6 Å FWHM. An additional 40 spectra were provided to us by C. Moran (1999, private communication); these have a comparable spectral coverage but at a slightly better resolution of  $\sim$  3 Å FWHM. Seven spectra from the southern hemisphere are taken from the analyses of Bragaglia et al. (1995) and Bergeron et al. (2001). Finally, high signal-to-noise ratio (S/N) optical spectra for 36 objects were obtained specifically for the purpose of this project during four observing runs in 2003 and 2004, using again the Steward Observatory facility.

## 2.2. Fitting Procedure

The method used for fitting the spectroscopic observations relies on the so-called spectroscopic technique developed by Bergeron et al. (1992a), and which has been refined by B95 and more recently by Liebert et al. (2005, LBH hereafter). The most important improvement of the method is the way the continuum used to normalize individual Balmer lines is defined. The approach is slightly different depending on the temperature range in question. For stars in the interval  $16,000 \gtrsim T_{\rm eff} \gtrsim 9000$  K, pseudo-Gaussian profiles are used whereas outside this temperature range synthetic spectra are utilized to determine the continuum (see Fig. 4 of LBH). Once the Balmer lines are normalized properly, we proceed to fit them with a grid of synthetic spectra derived from model atmospheres with a pure hydrogen composition. Our grid covers a range between  $T_{\rm eff} = 1500$  K and 140,000 K by steps of 500 K at low temperatures ( $T_{\rm eff} < 17,000$  K) and 5000 K at high temperatures ( $T_{\rm eff} > 20,000$  K), and a range in log g between 6.5 and 9.5 by steps of 0.5 dex (steps of 0.25 dex are used between 8000 K and 17,000 K where Balmer lines reach their maxima). For models where convective energy transport becomes important, we adopt the ML2/ $\alpha = 0.6$  parametrization of the mixing-length theory, as prescribed by B95.

One of the trickiest aspects of fitting optical spectra near the ZZ Ceti instability strip

is the fact that we overlap the temperature interval over which the equivalent widths of the Balmer lines reach their maximum near  $T_{\rm eff} \sim 13-14,000$  K (see, e.g., Fig. 4 of B95). Hence, in some cases, the minimization procedure allows two acceptable solutions, one on each side of this maximum. When the true effective temperature of the star is more than  $\sim 2000$  K away from the maximum, it is possible from a simple visual inspection of the fits to discriminate between the cool and the hot solutions. Indeed, for identical equivalent widths, the Balmer lines on the cool side of the maximum have deeper line cores. For stars in the range  $T_{\rm eff} \sim 11,500-16,000$  K we rely on the slopes of the observed and theoretical spectra normalized to unity at 4600 Å to discriminate between both solutions. As the slope of the energy distribution changes rapidly with temperature, it becomes relatively easy to decide which solution to adopt. Finally, whenever possible, our choice of solution has been confirmed by comparing multichannel, Strömgren, or Johnson photometry published in McCook & Sion (1999) with the theoretical color predictions of Bergeron et al. (1995b).

LBH used multiple spectroscopic observations of individual white dwarfs to estimate the external uncertainties of the fitted atmospheric parameters obtained from the spectroscopic technique (see their Fig. 8). Their estimate of the external error of each fitted parameter is 1.2% in  $T_{\rm eff}$  and 0.038 dex in  $\log g$ . We adopt the same uncertainties in this analysis since both data sets are identical in terms of data acquisition, reduction, and S/N.

## 2.3. Results

# 2.3.1. Adopted Atmospheric Parameters

The values of  $T_{\rm eff}$  and  $\log g$  for each of the 121 constant DA stars are listed in Table 1. We also include masses and absolute visual magnitudes derived from the evolutionary models of Wood (1995) with carbon-core compositions, helium layers of  $q({\rm He}) \equiv M_{\rm He}/M_{\star} = 10^{-2}$ , and thick hydrogen layers of  $q({\rm H}) = 10^{-4}$ . Several individual objects in Table 1 are worth discussing before looking at the global properties of the sample.

There are four known unresolved double degenerates included in our sample. The first three of those are G1-45 (WD 0101+048; Maxted et al. 2000), and LP 550-52 (WD 1022+050) and G21-15 (WD 1824+050; Maxted & Marsh 1999). Liebert et al. (1991) have shown that in such cases the atmospheric parameters derived are in fact an average of the parameters of both components of the system. Similarly, Bergeron et al. (1990a) suggested on the basis of spectroscopic and energy distribution fits that GD 387 (WD 2003+437) is probably composed of a DA and a DC star. They derived  $T_{\rm eff} = 14,340$  K and  $\log g = 7.50$  for the DA component. Therefore, the atmospheric parameters reported here for these four systems

are quite uncertain.

Three stars in Table 1 have composite spectra, and reprocessing of the EUV flux from the white dwarf primary in the chromosphere of the secondary contaminates the center of some, or all, of the Balmer lines. These are PG 0308+096 (Saffer et al. 1993), PG 1643+144 (Kidder 1991) and Case 1 (WD 1213+528; Lanning 1982). For PG 0308+096, the only contaminated line is H $\beta$ . Therefore, we exclude that line from the fitting procedure and are able to get a satisfactory fit with atmospheric parameters identical to those reported in Table 2 of LBH. Similarly, in the case of PG 1643+144 we exclude both H $\beta$  and H $\gamma$ . For Case 1 however, nearly all the spectral lines, and H $\beta$  in particular, are contaminated by the companion. As before, we exclude H $\beta$  but we also exclude 25 Å from either side of the line centers for H $\gamma$  through H $\epsilon$ , fitting only the line wings of the Balmer series. The effective temperature thus obtained,  $T_{\rm eff}=13,920$  K agrees well enough with that determined by Sion et al. (1984) based on a fit of to the IUE spectrum,  $T_{\rm eff}=13,000\pm500$  K,

Finally, our sample also includes two stars known to be magnetic, GD 77 (WD 0637+477; Schmidt et al. 1992) and G128-72 (WD 2329+267; Moran et al. 1998). They both show the characteristic Zeeman splitting of the Balmer lines caused by their magnetic fields and thus fitting their spectra is problematic due to the additional spectral broadening. Therefore the atmospheric parameters reported here for these two objects remain uncertain. For instance we obtain for G128-72 a spectroscopic solution of  $T_{\rm eff}=11,520$  K and  $\log g=9.09$ , while a fit to the BVRIJHK photometric energy distribution combined with a trigonometric parallax measurement yields  $T_{\rm eff}=9400$  K and  $\log g=8.02$  according to Bergeron et al. (2001).

These uncertain atmospheric parameter measurements are indicated by colons in Table 1 and we must pay particular attention to the corresponding objects when discussing the ZZ Ceti instability strip below.

#### 2.3.2. G226-29

Before discussing the results of our analysis any further, we want to consider the case of G226-29. Being the hottest ZZ Ceti star analyzed by Bergeron et al. (2004) with  $T_{\rm eff}$  = 12, 460 K and log g=8.28, G226-29 represents an important object for determining the slope of the blue edge of the ZZ Ceti instability strip (see Fig. 4 of Bergeron et al. 2004). These atmospheric parameter determinations are based on the same spectrum than the one used by B95 in their analysis of the atmospheric convective efficiency in DA white dwarfs. However, B95 also discuss a second spectroscopic observation of G226-29 with derived atmospheric parameters that agree within the uncertainties with the values given above. To be more

specific, the atmospheric parameters derived from this second observation are  $T_{\rm eff}=12,260~{\rm K}$  and  $\log g=8.32$ , consistent with the previous estimates within the uncertainties quoted in the previous section. What is more interesting perhaps is that this new temperature estimate is now in perfect agreement with the UV temperature obtained from the IUE spectrum,  $T_{\rm eff}=12,270~{\rm K}$  (see Fig. 12 of B95). Given this improved internal consistency, we adopt from now on these new atmospheric parameters for G226-29. These are reported in Table 2 together with the values for the mass and absolute magnitude.

# 2.3.3. New ZZ Ceti Stars

To complete the picture, in addition to the nonvariable stars given in Table 1, we need to include all ZZ Ceti stars for which we have spectroscopic observations. These include the 36 ZZ Ceti stars from Bergeron et al. (2004) as well as 3 new ZZ Ceti stars: PB 520 and GD 133 discovered by Silvotti et al. (2005) and Silvotti et al. (2005, in preparation), respectively, and G232-38 (WD 2148+539; V = 16.4) discovered as part of our ongoing spectroscopic survey of the McCook & Sion catalog described in § 4. Our fits to the Balmer lines of these new variables are presented in Figure 1; the atmospheric parameters for each object are reported in Table 2 together with the masses and absolute visual magnitudes. The values of  $T_{\rm eff}$  and  $\log g$  place PB 520 and G232-39 squarely within the limits of the ZZ Ceti instability strip (see Fig. 6 below) and we were more than confident that high speed photometric measurements would confirm their variability.

Silvotti et al. (2005) had already reported the detection of photometric variability in PB 520. G232-38, on the other hand, had never been observed before for photometric variability to our knowledge. Thus, we obtained high-speed photometric observations of G232-38 during an observing run in 2004 October at the 1.6 m telescope of the Observatoire du mont Mégantic equipped with LAPOUNE, the portable Montréal three-channel photometer. In all, we were able to obtain 3.9 h of data. Our sky-subtracted, extinction-corrected light curve of G232-38 is displayed in Figure 2. G232-38 is clearly a ZZ Ceti star with multiperiodic luminosity variations. The resulting Fourier (amplitude) spectrum is displayed in Figure 3. Three main-frequency components are easily discernible, with periods of 741.6, 984.0 and 1147.4 s. These relatively long periods and the rather large amplitude ( $\lesssim 10\%$ ) of the luminosity variations are consistent with the location of G232-38 somewhat closer to the red edge of the ZZ Ceti instability strip (see below).

After this paper was submitted, it has come to our attention that GD 133 (WD 1116+026) has been identified as a short period ( $\sim 120 \text{ s}$ ), low-amplitude (< 1%) ZZ Ceti star by Silvotti et al. (2005, in preparation) based on high-speed photometric observations obtained

at the VLT with ULTRACAM. This object has long been thought to be photometrically constant according to numerous published sources (McGraw 1977; Kepler et al. 1995; Giovannini 1996; Silvotti et al. 1997). Back in March 2003, two of us (G.F. and P.B.) had even observed this star with the 61-inch telescope at the Mount Bigelow observatory, the light curve of which is displayed in Figure 4. Although there is no obvious periodicity observed in the light curve, the corresponding Fourier (amplitude) spectrum shown in Figure 5 yields one significant peak above the  $1\sigma$  noise level with a period of 120.13 s, consistent with the observations of Silvotti et al. We have two independent optical spectra for GD 133, one from C. Moran (1999, private communication) that yields  $T_{\text{eff}} = 12,090 \text{ K}$  and  $\log g = 8.06$ , and our own data obtained in 2003 June that yields  $T_{\text{eff}} = 12,290 \text{ K}$  and  $\log g = 8.05$ . Although both sets of atmospheric parameters are consistent within the uncertainties, the former solution places GD 133 within the confines of our empirical instability strip and this is the solution we will adopt here. We report the atmospheric parameters for GD 133 in Table 2 along with our determination for the mass and absolute visual magnitude. We note that the location of GD 133 at the blue edge of the strip (see Fig. 6 below) is entirely consistent with the low amplitude and short pulsation period observed in Figures 4 and 5.

# 2.3.4. The Empirical ZZ Ceti Instability Strip

The locations of all 121 constant DA stars from Table 1 along with the 36 ZZ Ceti stars from Bergeron et al. (2004) and the 3 new ZZ Ceti stars discussed above are plotted in Figure 6 in a  $T_{\rm eff} - \log g$  diagram. Only 82 out the 121 nonvariables have atmospheric parameters that place them within the confines of Figure 6. The bold open circles within the strip correspond, from left to right, to the new ZZ Ceti stars GD 133, PB 520, and G232-38.

Given this unbiased sample, we can clearly see that the ZZ Ceti stars define a trapezoidal region in the  $T_{\rm eff}$ -log g plane in which no nonvariable stars are found, within the measurement errors, in agreement with the conclusions of Bergeron et al. (2004) and references therein. And there is certainly no need here to go through any statistical analysis to conclude that the ZZ Ceti instability strip is indeed pure. We must also note that all nonvariable white dwarfs claimed to be close or even within the ZZ Ceti instability strip are in fact well outside the strip according to our analysis. These are GD 52 (WD 0348+339; Dolez et al. 1991; Silvotti et al. 1997); G8-8 (WD 0401+250; Silvotti et al. 1997; Kepler & Nelan 1993); GD 31 (WD 0231-054), Rubin 70 (WD 0339+523), GD 202 (WD 1636+160) according to Dolez et al. (1991); PB 6089 (WD 0037-006) and G130-5 (WD 2341+322) according to Silvotti et al. (1997); BPM 20383 (WD 1053-550), BPM 2819 (WD 0255-705) according to Kepler & Nelan (1993, PG 1022+050 is a double degenerate); PG 1119+385, GD 515 (WD 1654+637),

GD 236 (WD 2226+061) according to Kepler et al. (1995). There is also the case of GD 556 (WD 2311+552; Dolez et al. 1991; Kepler et al. 1995; Giovannini et al. 1998), which we find slightly hotter than the red edge of the strip; this object is discussed further in the next section.

One of the primary goals of our study is to improve the determination of the location of the blue and red edges of the empirical ZZ Ceti instability strip by using both variable and nonvariable DA white dwarfs. The results shown in Figure 6 first reveal that the location of the red edge is better constrained than the blue edge, in particular because of the three nonvariables (GD 556, GD 426, and EC 12043-1337) that lie very close to the red edge. In contrast, there are very few hot nonvariables near the blue edge. Note that the filled squares at the top of the figure are unresolved double degenerates and the atmospheric parameters obtained here are the average values of both components of the system. Hence these cannot be used to constrain the slope of the blue edge. In addition, our revised temperature for G226-29, which is 200 K cooler than our previous estimate, now removes the previous constraint we had on the slope of the blue edge. We show in Figure 6 the range of possibilities for the blue edge as defined by our spectroscopic analysis. It is clear that additional observations close to the blue edge are badly needed to constrain the slope better.

We point out, in this connection, that nonadiabatic pulsation theory does suggest that the slope of the blue edge in a  $T_{\rm eff}$  –  $\log g$  diagram such as the one shown in Figure 6 should be significantly smaller than that of the red edge, leading to an expected strip which is wider at higher surface gravities. The last word on the question of the theoretical ZZ Ceti instability strip has been presented by Fontaine et al. (2003). We show in Figure 6 an updated comparison with their theoretical results (solid lines). We find that the slope of the theoretical blue edge is compatible with the range of possibilities allowed by our empirical results. On the other hand, the slope of the theoretical red edge is not too different from our own determination however it is predicted to be somewhat hotter than the red edge inferred from observation. Our aim in the future is to focus on the *empirical* boundaries with improved statistics, especially for the blue edge.

A global characteristic that is also noticeable in Figure 6 is the trend toward higher values of  $\log g$  as  $T_{\rm eff}$  decreases. This is now a familiar result observed in all spectroscopic surveys extending to low temperatures (B95, Koester et al. 2001, Kleinman et al. 2004, LBH, Gianninas et al. 2005). It has been proposed by Bergeron et al. (1990b) that these high inferred masses could be the result of small amounts of helium brought to the surface by the hydrogen convection zone, hence increasing the atmospheric pressure. When analyzed with pure hydrogen models, this increased pressure could be misinterpreted as resulting from of a high mass (see also Boudreault & Bergeron 2005).

## 2.3.5. GD 556

One constant star in Figure 6, GD 556, has an effective temperature slightly hotter than the empirical red edge. If we refer to Table 1, there are four independent sources that concluded that GD 556 is not a variable DA white dwarf. However, we would like to recall that initially G30-20 had also been found to be constant by Dolez et al. (1991) and Bergeron & McGraw (1989, unpublished) but was later identified as a ZZ Ceti pulsator by Mukadam et al. (2002); GD 133 discussed above is also a good example. It is worth mentioning that GD 556 presents certain challenges as far as photometric observations are concerned. Firstly, it is a rather dim star with  $V \sim 16.2$  (McCook & Sion 1999). Secondly, its position near the red edge implies that if it is indeed a pulsator, it should show long period pulsations that can be difficult to detect if one observes the star while two pulsational modes are interfering destructively. Considering all these facts, we believe that GD 556 is definitely worth re-observing under favorable conditions, both photometrically and spectroscopically. Nonetheless, if GD 556 truly is photometrically constant, then considering our error bars, the fact that it lies within the strip, albeit very close to the red edge, changes nothing in our conclusions relative to the the purity of the ZZ Ceti instability strip.

# 3. RESULTS FROM THE SLOAN DIGITAL SKY SURVEY

Since the discovery of the first pulsating DA white dwarf by Landolt (1968), HL Tau 76, and up to the spectroscopic study of Bergeron et al. (2004), a total of 36 ZZ Ceti stars were known (see Table 1 of Bergeron et al. 2004), a quarter of which had been discovered using the spectroscopic technique. In a single effort, Mukadam et al. (2004a) reported the discovery of 35 new ZZ Ceti pulsators, hence nearly doubling the number of known variables in this class. Thirty three of these have been discovered in the white dwarf SDSS sample, mostly from the first data release (Kleinman et al. 2004), and two more from the Hamburg Quasar Survey. Very recently, Mullally et al. (2005) reported the discovery of eleven more ZZ Ceti stars from SDSS as well as several nonvariable stars. However, the stars from Mullally et al. (2005) are not included in the analysis and discussion that follow.

ZZ Ceti candidates from the SDSS were selected for follow-up high-speed photometry on the basis of various techniques including ugriz photometry, equivalent width measurements, and the spectroscopic technique using SDSS spectra and Koester's model atmospheres. By far, the spectroscopic technique led to a significantly higher success rate of discovery than other techniques (90% by confining the candidates between  $T_{\rm eff} = 11,000$  K and 12,000 K). The 33 new SDSS pulsators are listed in Table 1 of Mukadam et al. (2004a), while nonvariables are given in their Tables 2 and 3 for different detection thresholds. An examination of

these tables reveal that all objects are relatively faint ( $g \gtrsim 17$ ) due to the intrinsic characteristics of the Sloan survey, which is aimed at identifying distant galaxies and quasars. Stellar objects on a given plate with an assigned fiber had to be faint in order not to saturate the detector.

Even though effective temperatures and surface gravities obtained from spectroscopic fits were provided in their paper, Mukadam et al. (2004a) did not discuss the implications of their new discoveries on the empirical determination of the ZZ Ceti instability strip. That discussion was deferred to a second paper by Mukadam et al. (2004b) who analyzed in more detail the spectroscopic results from their first paper, with a particular emphasis on the empirical ZZ Ceti instability strip as inferred from the location of variables and nonvariables in the  $T_{\rm eff} - \log g$  plane. In particular, the authors of that study question one more time the purity of the ZZ Ceti instability strip. The results of their analysis are contrasted with our results in Figure 7. We should mention that both analyses rely on different sets of model atmospheres (ours versus D. Koester's models) and there could be systematic offsets. But the most striking feature of the Mukadam et al. results is the large number of nonvariable white dwarfs within their empirical instability strip.

Through a painstaking statistical analysis of their results, Mukadam et al. (2004b) conclude that 18 nonvariables fall within the ZZ Ceti instability strip. Given that 33 new pulsators have been discovered from the same sample, the results suggest that the ZZ Ceti instability strip is only  $\sim 50\%$  pure, at best. The authors have even estimated the probability that the instability strip is pure is only 0.004 %! This result is of course in sharp contrast with our conclusions based on a comparable number of white dwarfs, and considerably brighter than those discovered in the SDSS. If indeed the instability strip is contaminated by a significant fraction of nonvariables, as implied by Mukadam et al., then the global properties of DA stars inferred from asteroseismological studies of ZZ Ceti stars could not be generalized to the entire population of hydrogen-atmosphere white dwarfs as the ZZ Ceti pulsators would no longer represent a phase through which all DA stars must evolve. Another important implication of this challenging result is that the pulsation instability of a white dwarf would no longer depend solely on its effective temperature and stellar mass, but would require an additional, yet unidentified, physical parameter to discriminate variables and nonvariables within the instability strip.

How can our results be reconciled with those of Mukadam et al.? The authors claim that since the discovery of white dwarf variables in 1968, their study represents the first analysis of a homogeneous set of spectra acquired using the same instrument on the same telescope, and with consistent data reductions. There is even an implicit suggestion that this homogeneity could account for the fundamental difference between their analysis and that of

Bergeron et al. (2004). However, this point of view completely ignores the incentive behind the earlier study of B95 whose specific goal was to provide an analysis of a homogeneous set of spectroscopic observations of the 18 ZZ Ceti stars known at that time, observable from the northern hemisphere. As discussed in § 2.1 and 2.2 of B95, the first spectroscopic analysis of a sizeable sample of ZZ Ceti stars by Daou et al. (1990) relied on spectra acquired as part of a backup project by various observers, and thus with different telescopes, spectrographs, detectors, and reduction procedures. As such, the spectroscopic sample of Daou et al. was somewhat inhomogeneous. To overcome precisely this problem, it was deemed necessary for B95 to reacquire optical spectra for the ZZ Ceti stars using the same instrument setup and reduction techniques. Hence high S/N spectroscopic observations for the 18 ZZ Ceti stars were acquired using the 2.3-m telescope at Steward Observatory, equipped with the Boller & Chivens spectrograph and a Texas Instrument CCD detector; spectra of four additional ZZ Ceti stars from the southern hemisphere have also been analyzed by Bergeron et al., but even though the spectra were of comparable quality to those obtained at the Steward Observatory, these four stars were treated separately throughout their analysis to preserve the homogeneity of the spectroscopic sample.

Note that the same instrument setup has been used ever since in many of our studies, and in particular in the recent extensive spectroscopic analysis of LBH who reported effective temperatures and surface gravities for nearly 350 DA stars drawn from the Palomar Green (PG) Survey. Even though the completeness of the PG survey remains questionable, the sample analyzed by Liebert et al. represents one of the largest statistically significant samples of DA stars analyzed to date. Yet, only one ZZ Ceti candidate (PG 1349+552) was found within the empirical instability strip together with 9 previously known ZZ Ceti stars. Highspeed photometric observations by Bergeron et al. (2004) confirmed that PG 1349+552 was indeed a new ZZ Ceti pulsator. Hence the conclusions of LBH are consistent with those of Bergeron et al. (2004), with the results presented in this paper, and with the results of our ongoing survey of the McCook & Sion catalog discussed in § 4, that the empirical instability strip contains no nonvariable stars. Hence, arguments based on the homogeneity of the spectroscopic analyses are unlikely to be able to explain the discrepancy between our conclusions and the contrasting results of Mukadam et al. (2004b). If anything, a spectroscopic analysis of an inhomogeneous data set should lead to a contamination of the instability strip with nonvariables, not the other way around!

Mukadam et al. (2004b) also suggested that their analysis effectively samples a different population of stars, more distant by a factor of 10 than that of the Bergeron et al. (2004) sample. Actually, taking a median value of  $g \sim 18.5$  (see Fig. 8 below) and an absolute magnitude of  $M_g = 11.64$  obtained from a model atmosphere at  $T_{\rm eff} = 12,000$  K and  $\log g = 8$ , we derive a distance of only 230 pc, still relatively close by. There is really no

astrophysical reason to expect white dwarfs at that distance to behave differently from those at shorter distances. Other explanations must thus be sought.

A close examination of the 18 nonvariables claimed to be within the instability strip by Mukadam et al. (2004b, see their Table 1) reveals that all objects are among the faintest in their SDSS sample, as can be seen from Figure 8 where the distribution of SDSS white dwarfs taken from Tables 1 to 3 of Mukadam et al. (2004a) is shown as a function of the g magnitude in the ugriz photometric system. As discussed by B95, the S/N of the spectroscopic observations is one of the key aspects of the spectroscopic technique for determining precise atmospheric parameters, the other important one being the flux calibration. Since the exposure time of a given SDSS spectrum is set by that of the entire plate, the corresponding S/N must necessarily be a function of the magnitude of the star. To verify this assertion, we have measured the S/N values<sup>1</sup> of all SDSS spectra taken from Mukadam et al. (2004a), and plotted these values against the corresponding g magnitude. This is shown in Figure 9. As expected, fainter stars have lower S/N spectra, and only objects brighter than  $q \sim 17$ have S/N above 40. This is not the case with standard slit spectroscopy, however, where the exposure time can be adjusted on a star-to-star basis. In B95 for instance, the exposure times were set to achieve an imposed lower limit of  $S/N \sim 80$ , although most spectra had  $S/N \gtrsim 100$  since the exposure times were also set long enough to cover several pulsation cycles (for an average of  $\sim 4.8$  cycles) in order to obtain meaningful time-averaged spectra. We mention that this last criterion is not necessarily met in the SDSS spectroscopic data.

We now turn to a more detailed comparison of S/N between our spectroscopic sample and that of Mukadam et al. (2004a). We show in the top panel of Figure 10 the distribution of S/N values for our spectroscopic sample, including the photometrically constant stars from Table 1, the 36 ZZ Ceti stars from Bergeron et al. (2004), and the 3 new pulsators from Table 2. Out of 39 ZZ Ceti stars, 12 have spectra with an admittedly lower S/N value than the imposed lower limit of  $\sim$  80 set by B95 in their analysis. These spectra correspond to data provided to us by C. Moran (1999, private communication) in the course of his search for double degenerate binaries, or to spectroscopic observations obtained prior to the discovery of the photometric variability of the object; this includes the two ZZ Ceti stars PB 520 and G232-38 analyzed in this paper. Still, only two ZZ Ceti stars have spectra with S/N < 50, and none below 40. The spectra for our photometrically constant sample also have fairly high S/N values, almost all above 50. In contrast, the S/N of the SDSS spectra shown in the bottom panel of Figure 10 have considerably lower values, with most spectra

 $<sup>^1\</sup>mathrm{Here}$  the S/N is measured in the continuum between 4450 and 4750 Å.

<sup>&</sup>lt;sup>2</sup>Only a fraction of the SDSS spectra could be recovered from the SDSS Web site.

having S/N < 60. Even worse, the subsample of nonvariables claimed to lie within the instability strip (hatched histogram) has even lower S/N values, with most objects having S/N < 40. Hence, it is perhaps not too surprising that the results of Mukadam et al. (2004b) regarding the purity of the ZZ Ceti instability strip, which are based on an analysis of low S/N spectra, differ so much from our own conclusions based on much higher quality spectroscopic observations.

We illustrate in Figure 11 a typical spectrum from our own sample of ZZ Ceti stars, GD 66 with S/N = 80, and one from the SDSS sample, SDSS J084746.81+451006.3 with S/N = 20. The S/N value of the latter is actually more typical of the sample of nonvariables found within the strip (bottom panel of Fig. 10). It is clear that the spectroscopic solution will necessarily depend on the quality of these spectra. To quantify this assertion, we performed a Monte Carlo simulation by taking a series of model spectra at  $T_{\rm eff} = 12,000$  K and  $\log q = 8.0$ , by adding random noise to achieve a given signal-to-noise ratio, and by fitting these spectra with our standard fitting procedure. The resulting  $T_{\text{eff}}$  and  $\log g$  values are then used to compute the standard deviations  $\sigma_{T_{\rm eff}}$  and  $\sigma_{\log g}$  for this assumed S/N value. Values of S/N from 10 to 200 were explored, thus encompassing the entire range exhibited by the spectra analyzed in this paper and by Mukadam et al. (2004b). The results of this exercise are displayed in Figure 12. It is clear that stars with low S/N spectra will yield atmospheric parameters with larger internal uncertainties than those derived from higher quality observations. In particular, if we again take S/N = 20 as indicative of the SDSS stars, we see from Figure 12 that such spectra would yield effective temperatures that are uncertain by  $\sim 500$  K. If we consider that the width of the empirical instability strip is  $\sim 1000$  K, it is easy to understand how lower quality spectra could easily place non-variable stars within the strip and vice-versa. Furthermore, stars with  $S/N \sim 80$ , typical of our photometric sample, exhibit uncertainties of roughly 150 K, which is entirely consistent with the uncertainties quoted in §2.2. Thus despite the homogeneous characteristics of the SDSS spectra in terms of instrument, telescope, and data reductions, their typical S/N is most likely too low to allow a precise measurement of the atmospheric parameters for these stars, or to determine accurately the location of the empirical ZZ Ceti instability strip, or to assess the purity of the strip for that matter.

Finally, we examine in Figure 13 the location of the SDSS white dwarfs in the  $T_{\rm eff}$  – log g plane. In each panel we consider only the objects with spectra above a certain threshold in S/N (the bottom panel includes all objects). Also reproduced is the empirical ZZ Ceti instability strip determined by Bergeron et al. (2004). The top panel with S/N > 70 corresponds to a threshold that would include  $\sim 80\%$  of all ZZ Ceti stars from the sample of Bergeron et al. (2004, top panel of Fig. 10). By comparison, only 2 objects from the SDSS sample meet this criterion. Hence if we restrict the analysis to the best spectra of both samples, the re-

sults are consistent: all variables are found within the empirical strip and all nonvariables lie outside. For S/N > 40 (middle panel), 9 objects from the SDSS sample are found in the temperature range shown in Figure 13. In this case, however, one variable star (WD 1711+6541 at  $T_{\rm eff}=11,310~{\rm K}$  and  $\log g=8.64$ ) falls slightly below the empirical red edge of the strip, while one nonvariable star (WD 1338-0023 at  $T_{\rm eff}=11,650~{\rm K}$  and  $\log g=8.08$ ) sits comfortably near the middle of the strip. Since these two objects are relatively bright (g=16.89 and 17.09, respectively), we managed to secure our own spectroscopic observations of these stars using the Steward Observatory 2.3 m telescope during an observing run in 2004 May. Reassuringly enough, our independent analysis of these two objects in terms of both data and models —  $T_{\rm eff}=11,490~{\rm K}$  and  $\log g=8.56$  for WD 1711+6541 and  $T_{\rm eff}=11,980~{\rm K}$  and  $\log g=7.94$  for WD 1338-0023 — places them where they are expected, that is, inside and outside the instability strip, respectively (see Fig. 13).

For completeness, we show at the bottom of Figure 13 all the objects from the SDSS sample (S/N > 0). Once again, we can see that the bulk of this sample is characterized with S/N values below 40, the threshold value used in the middle panel, and that the conclusion about the purity of the ZZ Ceti instability strip rests heavily on the quality of the spectroscopic observations.

# 4. ONGOING SPECTROSCOPIC SURVEY

In order to increase the number of stars in our spectroscopic (and eventually photometric) sample, we have undertaken a broader spectroscopic survey of DA stars drawn from the Catalog of Spectroscopically Identified White Dwarfs of McCook & Sion (1999). We have defined our sample using the following criteria: (1) a temperature index lying between 3 and 7, (2) apparent visual magnitudes of V < 17 and (3) declination greater than -30 degrees. High S/N optical spectroscopic observations are currently being secured for each star that meets these criteria. This survey was initiated with several goals in mind. First and foremost, we wish to obtain measurements of  $T_{\rm eff}$  and  $\log g$  for each object. Secondly, we want to confirm the spectroscopic classification of stars from the catalog (we have already identified 29 stars misclassified as DA stars that are clearly lower gravity objects). A final goal of our survey is to identify new ZZ Ceti candidates (G232-38 has been discovered in this survey). This is the reason for restricting ourselves to stars with the aforementioned range of temperature indices. Some preliminary results of this analysis have already been presented in Gianninas et al. (2005). Among these is the discovery of a unique DAZ white dwarf, GD 362 (Gianninas et al. 2004).

The combined results of our ongoing spectroscopic survey and of the photometric sample

analyzed in § 2 are displayed in Figure 14 as triangles and circles, respectively. The three low-gravity objects in the vicinity of the instability strip are known double degenerate systems. We have already discussed two of these (see § 2.3.4 and Fig. 6), the third is GD 429 (Maxted et al. 2000) which has yet to be observed for photometric variability. We clearly see that many objects from our survey lie very close to both the red and blue edges of the instability strip. These stars are important as we attempt to determine better the exact boundaries of the instability strip. Therefore, we plan on securing high speed photometric observations for these objects in order to confirm their photometric status. These results will be reported in due time.

# 5. CONCLUSION

We have gathered optical spectra for 121 photometrically constant DA white dwarfs for which we derived values of  $T_{\rm eff}$  and  $\log g$ . Using these nonvariable white dwarfs together with a sample of 39 relatively bright ZZ Ceti stars, we wished to obtain a better understanding of the location and shape of the red and blue edges of the ZZ Ceti instability strip. In so doing, we have succeeded in better populating the  $T_{\rm eff}$ -log g plane in the vicinity of the ZZ Ceti instability strip. We find that the location and slope of the red edge is quite well constrained whereas our newly adopted atmospheric parameters for G226-29 allow for a much broader range of slopes for the blue edge which would accommodate our current photometric sample. Furthermore, we find no nonvariable white dwarfs within the ZZ Ceti instability. This supports our belief that ZZ Ceti stars represent an evolutionary stage by which all DA white dwarfs must pass.

The optical spectra that we analyzed were gathered as part of a more extensive survey of DA white dwarfs from the catalog of McCook & Sion (1999). This survey has several goals, among them, the identification of candidate ZZ Ceti stars. Thus far, two of these, PB 520 and G232-38, have been identified as ZZ Ceti pulsators by Silvotti et al. (2005) and us, respectively. The spectroscopic technique pioneered by B95 has proven once again to be an invaluable tool as far as identifying new candidate ZZ Ceti stars. Indeed, it has maintained its 100% success rate in predicting variability in DA white dwarfs. With the inclusion of PB 520, G232-38, and GD 133 the number of ZZ Ceti stars (excluding the SDSS stars) swells to 39 of which 11 have been successfully identified using this method. Even among the ZZ Ceti stars discovered through SDSS, the most fruitful method for identifying candidates was the spectroscopic method (Mukadam et al. 2004a). In the future, in order to define better the blue edge, and to study further the instability strip as a whole, we plan on securing high speed photometric observations for all the DA white dwarfs that are within or near the

boundaries of the empirical strip and that have never been observed for variability.

We have also been able to show the importance of using high-quality data (i.e., high S/N) when performing analyses such as these through an in-depth examination of the data used by Mukadam et al. (2004b) in their study. It is clear that their controversial results, which place a large number of nonvariable stars within the instability strip, can be traced back to spectra of lesser quality that greatly affect the result of the spectroscopic fit. However, one cannot discount the fact that Mukadam et al. (2004a) have nearly doubled the number of known ZZ Ceti stars as well as adding a large number of nonvariable DA white dwarfs to the mix. The study of the ZZ Ceti instability strip can only benefit from the inclusion of all recently identified variable and nonvariable DA white dwarfs within our sample. We are therefore exploring the possibility of obtaining high S/N optical spectra for all the DA white dwarfs from Mukadam et al. (2004a), Silvotti et al. (2005), and Mullally et al. (2005) in the near future.

We would like to thank the director and staff of Steward Observatory for the use of their facilities. We would also like to thank the director and staff of the Observatoire du mont Mégantic for the use of their facilities and for supporting LAPOUNE as a visitor instrument. We also acknowledge the contribution of F. Provencher in the analysis of the SDSS data. This work was supported in part by the NSERC Canada and by the Fonds Québécois de la recherche sur la nature et les technologies (Québec). GF acknowledges the contribution of the Canada Research Chair Program.

# REFERENCES

- Bergeron, P., Fontaine, G., Billères, M., Boudreault, S., & Green, E. M. 2004, ApJ, 600, 404
- Bergeron, P., Greenstein, J. L., & Liebert, J. 1990a, ApJ, 361, 190
- Bergeron, P., Leggett, S. K., & Ruiz, M. T. 2001, ApJS, 133, 413
- Bergeron, P., Liebert, J., & Fulbright, M. S. 1995a, ApJ, 444, 810
- Bergeron, P., Saffer, R. A., & Liebert, J. 1992a ApJ, 394, 228
- Bergeron, P., Wesemael, F., & Beauchamp, A. 1995b, PASP, 107, 1047
- Bergeron, P., Wesemael, F., Fontaine, G. 1992b, ApJ, 387, 288
- Bergeron, P., Wesemael, F., Fontaine, G., & Liebert, J. 1990b, ApJ, 351, L21
- Bergeron, P., Wesemael, F., Lamontagne, R., Fontaine, G., Saffer, R. A., & Allard, N. F. 1995c, ApJ, 449, 258 (B95)
- Boudreault, S., & Bergeron, P. 2005, in 14th European Workshop on White Dwarfs, ed. D. Koester & S. Moehler (San Francisco: ASP), in press
- Bragaglia, A., Renzini, A., & Bergeron, P. 1995, ApJ, 443, 735
- Daou, D., Wesemael, F., Bergeron, P., Fontaine, G., & Holberg, J. B. 1990, ApJ, 364, 242
- Dolez, N., Vauclair, G., & Koester, D. 1991, in Proceedings of the 7th European Workshop on White Dwarfs, NATO ASI Series, eds. G. Vauclair & E. Sion (Dordrecht: Kluwer), 361
- Fontaine, G., Bergeron, P., Lacombe, P., Lamontagne, R., & Talon, A. 1985, AJ, 90, 1094
- Fontaine, G., McGraw, J. T., Dearborn, D. S. P., Gustafson, J., & Lacombe, P. 1982, ApJ, 258, 651
- Fontaine, G., Brassard, P., & Charpinet, S. 2003, ApSS, 284, 257
- Fontaine, G., Tassoul, M., & Wesemael, F. 1984, in Theoretical Problems in Stellar Stability and Oscillations, 25th Liège Astrophysical Colloquium, ed. A. Noels & M. Gabriel (Liège: Presses Univ. Liège), 328
- Gianninas, A., Bergeron, P., & Dufour, P. 2005, in 14th European Workshop on White Dwarfs, ed. D. Koester & S. Moehler (San Francisco: ASP), in press

Gianninas, A., Dufour, P., & Bergeron, P. 2004, ApJ, 617, L57

Giovannini, O. 1996, Ph.D. thesis, Universidade Federal do Rio Grande do Sul, Brazil

Giovannini, O., Kepler, S. A., Kanaan, A., Wood, M. A., Claver, C. F., Koester, D. 1998, Baltic Astron., 7, 131

Greenstein, J. L. 1976, AJ, 81, 323

Greenstein, J. L. 1982, ApJ, 258, 661

Kanaan, A., Kepler, S. O., & Winget, D. E. 2002, A&A, 389, 896

Kepler, S. O., Giovannini, O., Kanaan, A., Wood, M. A., & Claver, C. F. 1995, Baltic Astron., 4, 157

Kepler, S. O., & Nelan, E. P. 1993, AJ, 105, 608

Kidder, K. M. 1991, Ph.D. thesis, University of Arizona, Tucson

Kleinman, S. J., et al. 2004, ApJ, 607, 426

Koester, D., Napiwotzki, R., Christlieb, N., Drechsel, H., Hagen, H.-J., Heber, U., Homeier, D., Karl, C., Leibundgut, B., Moehler, S., Nelemans, G., Pauli, E.-M., Reimers, D., Renzini, A., & Yungelson, L. 2001, A&A, 378, 556

Lamontagne, R., Wesemael, F., & Fontaine, G. 1987, in IAU Colloquium 95, The Second Conference on Faint Blue Stars, eds. A. G. Davis Philip, D. S. Hayes, & J. Liebert (Schenectady: L. Davis), 677

Lamontagne, R., Wesemael, F., Fontaine, G., Wegner, G., and Nelan, E. P. 1989, in IAU Colloq. 114, White Dwarfs, ed. G. Wegner (Berlin: Springer), 240

Landolt, A. U., 1968, ApJ, 153, 151

Lanning, H. H. 1982, ApJ, 253, 752

Liebert, J., Bergeron, P., & Holberg, J. B. 2005, ApJS, 156, 47 (LBH)

Liebert, J., Bergeron, P., & Saffer, R. A. 1991, in Proceedings of the 7th European Workshop on White Dwarfs, NATO ASI Series, eds. G. Vauclair & E. M. Sion (Dordrecht: Kluwer), 409

Maxted, P. F. L., & Marsh, T. R. 1999, MNRAS, 307, 122

Maxted, P. F. L., Marsh, T. R., & Moran, C. K. J. 2000, MNRAS, 319, 305

McCook, G. P., & Sion, E. M. 1999, ApJS, 121, 1

McGraw, J. T. 1977, Ph.D. thesis, University of Texas at Austin

McGraw, J. T. 1979, ApJ, 229, 203

Moran, C., Marsh, T. R., & Dhillon, V. S. 1998, MNRAS, 299, 218

Mukadam, A. S., Kepler, S. O., Winget, D. E., Bergeron, P. 2002, ApJ, 580, 429

Mukadam, A. S., et al. 2004a, ApJ, 607, 982

Mukadam, A. S., Winget, D. E., von Hippel, T., Montgomery, M. H., Kepler, S. O., & Costa, A. F. M. 2004b, ApJ, 612, 1052

Mullally, F., Thompson, S. E., Castanheira, B.G., Winget, D. E., Kepler, S. O., Eisenstein, D. J., Kleinman, S. J., & Nitta, A. 2005, ApJ, 625, 966

Saffer, R. A., Wade, R. A., Liebert, J., Green, R. F., Sion, E. M., Bechtold, J., Foss, D., & Kidder, K 1993, AJ, 105, 1945

Schmidt, G. D., Stockman, H. S., & Smith, P. S. 1992, ApJ, 398, L57

Silvotti, R., Bartolini, C., Cosentino, G., Guarnieri, A., & Piccioni, A. 1997, in 10th European Workshop on White Dwarfs, ed. J. Isern, M. Hernanz & E. Garcia-Berro (Dordrecht: Kluwer), 489

Silvotti, R., Voss, B., Koester, D., & Bruni, I. 2005, in 14th European Workshop on White Dwarfs, ed. D. Koester & S. Moehler (San Francisco: ASP), in press

Sion, E. M., Guinan, E. F., & Wesemael, F. 1984, ApJ, 279, 758

Tassoul, M., Fontaine, G., & Winget, D.E. 1990, ApJS, 72, 335

Weidemann, V., & Koester, D. 1984, A&A, 132, 195

Wesemael, F., Bergeron, P., Fontaine, G., & Lamontagne, R. 1991, in Proceedings of the 7th European Workshop on White Dwarfs, NATO ASI Series, eds. G. Vauclair & E. M. Sion (Dordrecht: Kluwer), 159

Wesemael, F., & Fontaine, G. 1985, ApJ, 228, 764

Wesemael, F., Lamontagne, R., & Fontaine, G. 1986, AJ, 91, 1376

- Winget, D.E., Van Horn, H.M., Tassoul, M., Hansen, C.J., Fontaine, G., & Carroll, B.W. 1982, ApJ, 252, L65
- Wood, M. A. 1995, in Proceedings of the 9th European Workshop on White Dwarfs, eds. D. Koester & K. Werner (Berlin: Springer), 41

This preprint was prepared with the AAS LATEX macros v5.2.

Table 1. Atmospheric Parameters of Photometrically Constant DA White Dwarfs

WD	Name	$T_{\rm eff}$ (K)	$\log g$	$M/M_{\odot}$	$M_V$	Sources
0005-163	G158-132	14160	7.79	0.50	11.03	1
0009 + 501	G217-37	6610	8.36	0.83	14.31	2
0011 + 000	G31-35	9640	8.16	0.70	12.53	3
0030 + 4444	G172-4	10370	8.20	0.73	12.33	3
0032 - 175	G226-135	9830	8.18	0.71	12.49	4
0033 + 016	G1-7	10980	8.83	1.12	13.27	5, 6
0037 - 006	PB 6089	14920	7.86	0.54	11.04	1, 2, 5, 7, 8
$0101 + 048^{a}$	G1-45	8530:	8.27:	0.77	13.17	4
0103 - 278	G269-93	13290	7.83	0.52	11.21	6, 9
0115 + 521	GD 275	10710	8.12	0.68	12.09	1
0135 - 052	L870-2	7280	7.85	0.51	13.18	4
0143 + 216	G94-9	9290	8.49	0.92	13.22	3
0148 + 467	GD 279	13430	7.93	0.57	11.33	3
0151 + 017	G71-41	12330	7.89	0.54	11.42	1, 6, 8
0208 + 396	G74-7	7340	8.10	0.66	13.49	2
0213 + 396	GD 25	9320	8.56	0.96	13.32	3
0231 - 054	GD 31	13550	8.66	1.02	12.46	3, 5
0238 + 333	KUV 02386+3322	13390	8.23	0.75	11.77	10
0243 + 155	PG 0243+155	16670	8.02	0.63	11.08	5
0255 - 705	BPM 02819	10560	8.10	0.66	12.11	3, 6, 11
0302 + 621	GD 426	11000	8.21	0.73	12.15	5
$0308 + 096^{b}$	PG 0308+096	25900	8.08	0.68	10.36	9
0326 - 273	LTT 1648	9250	7.86	0.52	12.24	2, 9
0332 + 320	G38-4	10370	8.13	0.68	12.21	3
0339 + 523	Rubin 70	12640	7.39	0.33	10.69	5, 6, 8, 9
0339 - 035	GD 47	12470	7.98	0.60	11.53	3, 5
0348 + 339	GD 52	14190	8.20	0.74	11.63	1, 7
0352 + 096	HZ 4	14030	8.19	0.73	11.64	11
0401 + 250	G8-8	12240	7.99	0.60	11.57	1, 5, 6, 7, 8, 11
0406 + 169	LB 227	15070	8.26	0.78	11.62	12
0407 + 179	HZ 10	13620	7.79	0.50	11.11	3
0418 + 153	LB 212	13480	7.99	0.61	11.41	5
0440 + 510	G175-46	8620	8.22	0.74	13.04	3
0453 + 418	GD 64	13660	7.68	0.44	10.94	3
0513 + 756	GD 433	13540	7.76	0.48	11.08	1, 5

Table 1—Continued

WD	Name	$T_{\rm eff}$ (K)	$\log g$	$M/M_{\odot}$	$M_V$	Sources
0518+005	GD 67	13340	7.88	0.55	11.28	3
0533 + 322	G98-18	10680	7.89	0.54	11.76	1, 5
$0637 + 477^{c}$	GD 77	14000:	8.21:	0.74	11.66	2
0710 + 216	GD 83	10480	8.07	0.65	12.09	3
0743 + 442	GD 89	14500	8.36	0.84	11.85	1
0816+387	G111-71	7700	8.07	0.64	13.26	4
0830 + 371	G115-9	9180	8.26	0.76	12.87	3
0839 - 327	LHS 253	9270	7.89	0.54	12.27	3
0913 + 442	G116-16	8680	8.20	0.72	12.98	3
0920 + 216	LB 3025	18000	7.83	0.53	10.66	5
0926-039	G161-36	12860	7.86	0.53	11.32	8
0928 - 713	BPM 05639	8580	8.28	0.78	13.16	3
0943 + 441	G116-52	12820	7.55	0.39	10.90	6, 8, 11
0950 + 077	PG 0950+078	14770	7.95	0.59	11.19	12
0950 - 572	BPM 19738	12400	7.68	0.44	11.13	3, 8
0955 + 247	G49-33	8620	8.30	0.79	13.18	3
0956 + 045	PG 0956+046	18150	7.81	0.52	10.62	5
$1022 + 050^{a}$	LP 550-52	11680:	7.64:	0.42	11.20	6, 8, 11
1026 + 023	LP 550-292	12500	7.95	0.58	11.49	1, 6, 8, 9
1046 + 281	Ton 547	12610	7.97	0.59	11.51	3, 7
1053-550	BPM 20383	13420	7.81	0.51	11.16	11
1101 + 364	PG 1101+364	13040	7.24	0.29	10.41	6, 9
1108 + 475	GD 129	12460	8.24	0.76	11.92	13
1119 + 385	PG 1119+386	16500	7.94	0.58	10.98	6
1122 + 546	GD 307	14380	7.83	0.52	11.06	1
1147+255	G121-22	10200	8.14	0.69	12.29	3, 6
1204 - 136	EC 12043-1337	11180	8.24	0.76	12.16	13
$1213 + 528^{b}$	Case 1	13920	8.16	0.71	11.60	11
1229 - 012	$HE\ 1229-0115$	19740	7.52	0.41	10.05	5, 7
1241 + 235	LB 16	26730	7.93	0.60	10.05	7
1244+149	G61-17	10680	8.06	0.64	12.02	6
1253 + 482	GD 320	13970	7.59	0.41	10.78	1, 8
1327 - 083	Wolf 485A	13920	7.86	0.54	11.17	1, 6, 8, 11, 14
1418 - 005	PG 1418-005	14290	7.82	0.51	11.06	6, 8
1431 + 153	PG 1431+154	13550	7.95	0.58	11.35	12

Table 1—Continued

WD	Name	$T_{\rm eff}$ (K)	$\log g$	$M/M_{\odot}$	$M_V$	Sources
1448+077	G66-32	14170	7.75	0.48	10.97	6, 8
1507 - 105	GD 176	10100	7.75	0.47	11.76	3, 6
1508 + 637	GD 340	10450	8.12	0.68	12.18	1
1510 + 566	G201-39	9240	8.13	0.68	12.63	3
1531 + 184	GD 186	13220	7.89	0.55	11.30	3
1537+651	GD 348	9740	8.15	0.69	12.47	3, 7
1539 - 035	GD 189	10080	8.30	0.79	12.59	3, 6
1544 - 377	L481-60	10580	8.09	0.66	12.09	8
1550 + 183	GD 194	14260	8.25	0.77	11.70	6
1555 - 089	G152-B4B	13960	7.83	0.52	11.12	6, 8
1606+422	Case 2	12690	7.74	0.47	11.17	2, 6, 8
1609 + 135	G138-8	9320	8.64	1.01	13.48	3
1636 + 160	GD 202	13620	7.81	0.51	11.13	5, 6
1637 + 335	G180+65	10150	8.17	0.71	12.35	3
1643+143 <sup>b</sup>	PG 1643+144	26850	7.91	0.60	10.02	12
1654+637	GD 515	15070	7.63	0.43	10.70	6
1655+215	G169-34	9310	8.20	0.73	12.72	2, 3
1706+332	G181-B5B	12960	7.80	0.50	11.21	3
1700+332 $1716+020$	G19-20	13210	7.77	0.49	11.13	3, 6, 8
1743 - 132	G154-85B	12300	7.88	0.54	11.42	3
1110 102	GIOT COD	12000	1.00	0.01	11.12	9
$1824 + 040^{a}$	G21-15	11970:	7.57:	0.39	11.06	5
1826 - 045	G21-16	9210	8.16	0.70	12.70	3
1827 - 106	G155-19	13300	7.63	0.42	10.93	8
1840 - 111	G155-34	10170	8.23	0.75	12.44	3, 6
1857 + 119	G141-54	9920	8.12	0.68	12.36	3, 6
1911+135	G142-B2A	13270	7.85	0.53	11.25	6, 9
1952 - 206	LTT 7873	13740	7.85	0.53	11.18	2, 3
1953 - 011	G92-40	7780	8.25	0.75	13.49	3
$2003+437^{a}$	GD 387	16910:	7.80:	0.51	10.73	1
2025 + 488	GD 390	10720	8.05	0.63	11.99	1
2029+183	GD 230	13090	7.79	0.49	11.18	3
2047 + 372	G210-36	14070	8.21	0.74	11.66	8
2059+190	G145-4	6980	8.42	0.86	14.18	$\frac{\circ}{2}$
2105-820	BPM 01266	10620	8.25	0.76	12.33	3, 6, 8, 11
2115 - 560	BPM 27273	9760	8.13	0.68	12.43	6

Table 1—Continued

WD	Name	$T_{\rm eff}$ (K)	$\log g$	$M/M_{\odot}$	$M_V$	Sources
2117+539	G231-40	13990	7.78	0.49	11.04	9
2124 + 550	G231-43	13340	8.34	0.82	11.95	3, 9
2126 + 734	G261-43	15290	7.84	0.53	10.97	6, 11
2136 + 229	G126-18	10210	8.10	0.67	12.23	6
2149 + 372	GD 397	13080	7.87	0.54	11.29	1, 6
2226 + 061	GD 236	15280	7.62	0.43	10.66	6
2246 + 223	G127-58	10650	8.80	1.10	13.32	3, 6
2258 + 406	G216-B14B	9860	8.23	0.75	12.55	6
2306 + 130	KUV 23060+1303	13250	7.92	0.56	11.34	9
2311 + 552	GD 556	11180	8.15	0.69	12.01	1, 5, 6, 8
2314 + 064	PB 5312	17570	7.98	0.61	10.93	1, 5
2322 + 206	PG 2322+207	13060	7.84	0.52	11.26	2, 9
$2329 + 267^{c}$	G128-72	11520:	9.09:	1.24	13.67	2, 3
2337 - 760	BPM 15727	13420	7.39	0.33	10.57	6
2341 + 322	G130-5	12570	7.93	0.57	11.45	1, 3, 5, 6, 7, 8
2351 - 335	LDS 826A	8850	8.27	0.77	13.02	2

<sup>&</sup>lt;sup>a</sup>Double degenerate

Note. — (1) G. Fontaine (1979-1984, unpublished); (2) P. Bergeron & J. T. McGraw (1989, unpublished); (3) McGraw (1977); (4) Kanaan et al. (2002); (5) G. Vauclair (1979-1999, unpublished), Dolez et al. (1991); (6) Kepler et al. (1995); (7) Silvotti et al. (1997); (8) Giovannini (1996); (9) P. Bergeron & G. Fontaine (1990, unpublished); (10) G. Fontaine & P. Bergeron (1999, unpublished); (11) Kepler & Nelan (1993); (12) Mukadam et al. (2004a); (13) G. Fontaine & P. Bergeron (2003, unpublished); (14) Wesemael & Fontaine (1985).

 $<sup>^{\</sup>rm b}{
m Composite}$  spectrum

 $<sup>^{\</sup>rm c}{\rm Magnetic}$ 

Table 2. Atmospheric Parameters of ZZ Ceti Stars

WD	Name	$T_{\rm eff}$ (K)	$\log g$	$M/M_{\odot}$	$M_V$
$   \begin{array}{r}     1039 + 412 \\     1116 + 026 \\     1647 + 591^{a} \\     2148 + 539   \end{array} $	GD 133 G226-29	11550 12090 12260 11350	8.10 8.06 8.31 8.01	0.66 0.64 0.80 0.61	11.85 11.70 12.10 11.76

<sup>&</sup>lt;sup>a</sup>Based on a new spectroscopic observation (see text).

- Fig. 1.— Model fits to the individual Balmer line profiles of GD 133, PB 520, and G232-38. The lines range from H $\beta$  (bottom) to H8 (top), each offset vertically by a factor of 0.2. Values of  $T_{\text{eff}}$  and log g have been determined from ML2/ $\alpha = 0.6$  models.
- Fig. 2.— Light curve of G232-38, observed in "white light" with LAPOUNE attached to the Observatoire du mont Mégantic 1.6 m telescope. Each point represents a sampling time of 10 s. The light curve is expressed in terms of residual amplitude relative to the mean brightness of the star.
- Fig. 3.— Fourier (amplitude) spectrum of the light curve of G232-38 in the 0-10 mHz bandpass. The spectrum in the region from 10 mHz to the Nyquist frequency is entirely consistent with noise and is not shown. The amplitude axis is expressed in terms of the percentage variations about the mean brightness of the star.
- Fig. 4.— Light curve of GD 133, observed in "white light" with LAPOUNE attached to the 61-inch telescope at the Mount Bigelow observatory. Each point represents a sampling time of 10 s. The light curve is expressed in terms of residual amplitude relative to the mean brightness of the star.
- Fig. 5.— Same as Figure 3 for GD 133 and in the bandpass 0-15 mHz. The dashed line represents the  $1\sigma$  noise level.
- Fig. 6.—  $T_{\rm eff}$  log g distribution for DA white dwarfs with high-speed photometric measurements. The open circles represent the 36 ZZ Ceti stars from Bergeron et al. (2004) as well as the three recent discoveries reported by (bold circles from left to right) Silvotti et al. (2005, in preparation, GD 133), Silvotti et al. (2005, PB 520) and in this paper (G232-38). The filled circles represent the photometrically constant DA stars from Table 1 with appropriate effective temperatures; while the filled squares correspond to unresolved double degenerate systems. The error bars in the upper right corner represent the average uncertainties of the spectroscopic method in the region of the ZZ Ceti stars. The dashed lines represent the empirical blue and red edges of the instability strip while the solid lines represent the theoretical boundaries of the instability strip as computed by Fontaine et al. (2003).
- Fig. 7.—  $T_{\rm eff} \log g$  distribution for DA white dwarfs with high-speed photometric measurements taken from this paper and from the analysis of Mukadam et al. (2004b). The open circles represent ZZ Ceti stars while filled circles correspond to photometrically constant stars.
- Fig. 8.— Number distribution of DA stars taken from Tables 1 to 3 of Mukadam et al. (2004a) as a function of the q magnitude (solid line histogram) compared with the distribution of

nonvariables claimed to lie within the ZZ Ceti instability strip (*hatched histogram*) taken from Table 1 of Mukadam et al. (2004b).

Fig. 9.— S/N of the spectroscopic observations of the DA stars from Tables 1 to 3 of Mukadam et al. (2004a) as a function of the g magnitude.

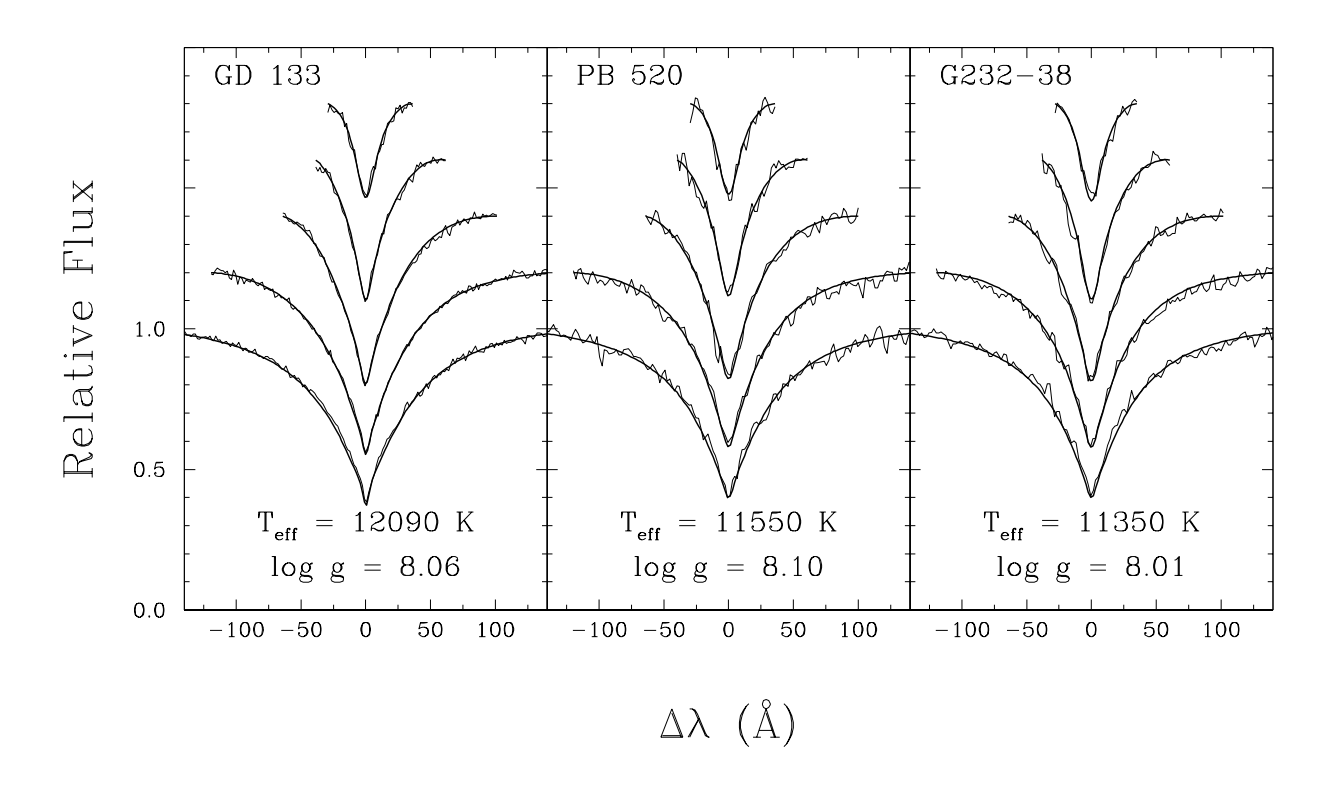
Fig. 10.— *Top:* Distribution of S/N for the 121 spectra of the photometrically constant stars from Table 1 (*solid line histogram*) and of the 36 ZZ Ceti stars from Bergeron et al. (2004) and the 3 additional ZZ Ceti stars from Table 2 (*hatched histogram*). *Bottom:* Same as the top panel but for 113 out of the 118 white dwarf spectra taken from Tables 1 to 3 of Mukadam et al. (2004a, *solid line histogram*), and for 17 out of the 18 nonvariables that lie within the ZZ Ceti instability strip according to Mukadam et al. (2004b, *hatched histogram*).

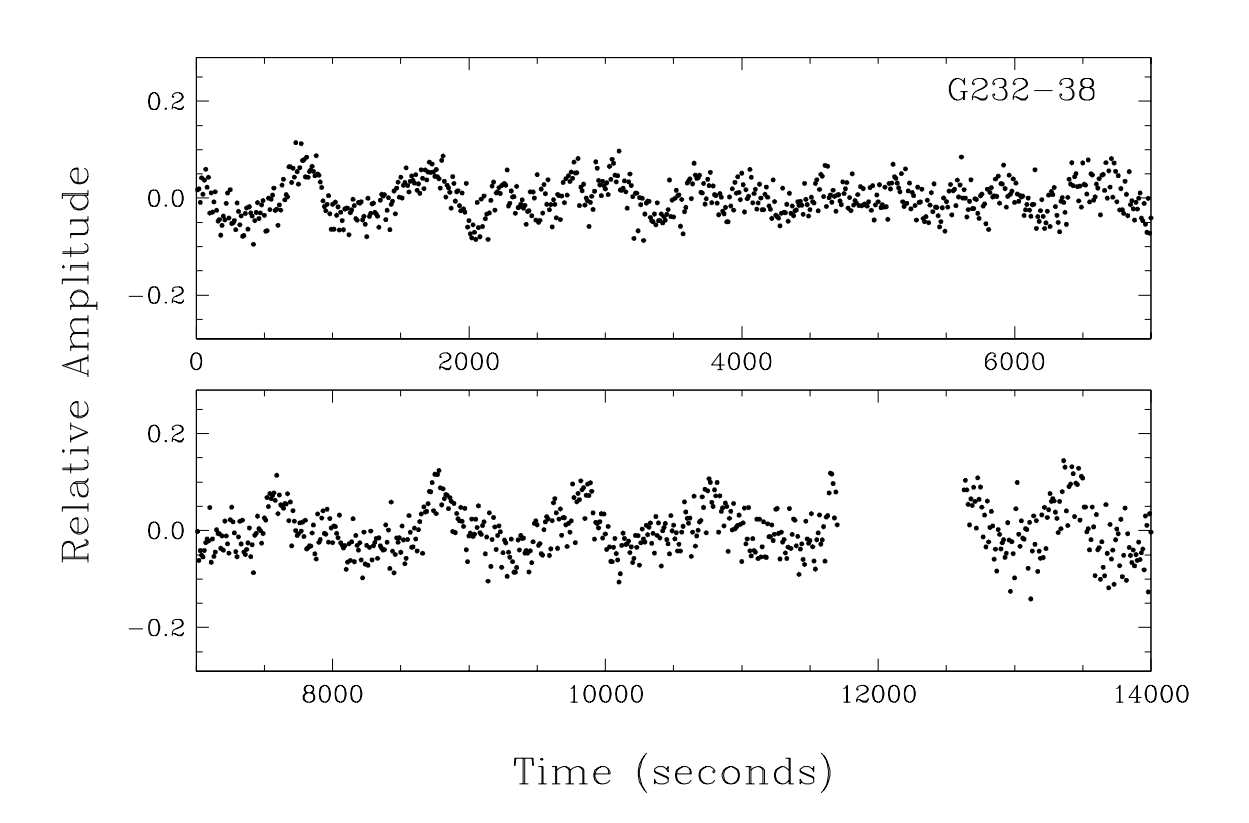
Fig. 11.— Typical ZZ Ceti spectra from the SDSS (top) and Bergeron et al. (2004, bottom). Both spectra are flux calibrated, normalized to unity at 4500 Å, and offset by a factor of 0.8 for clarity. The signal-to-noise ratio is S/N = 20 for SDSS J084746.81+451006.3 and S/N = 80 for GD 66.

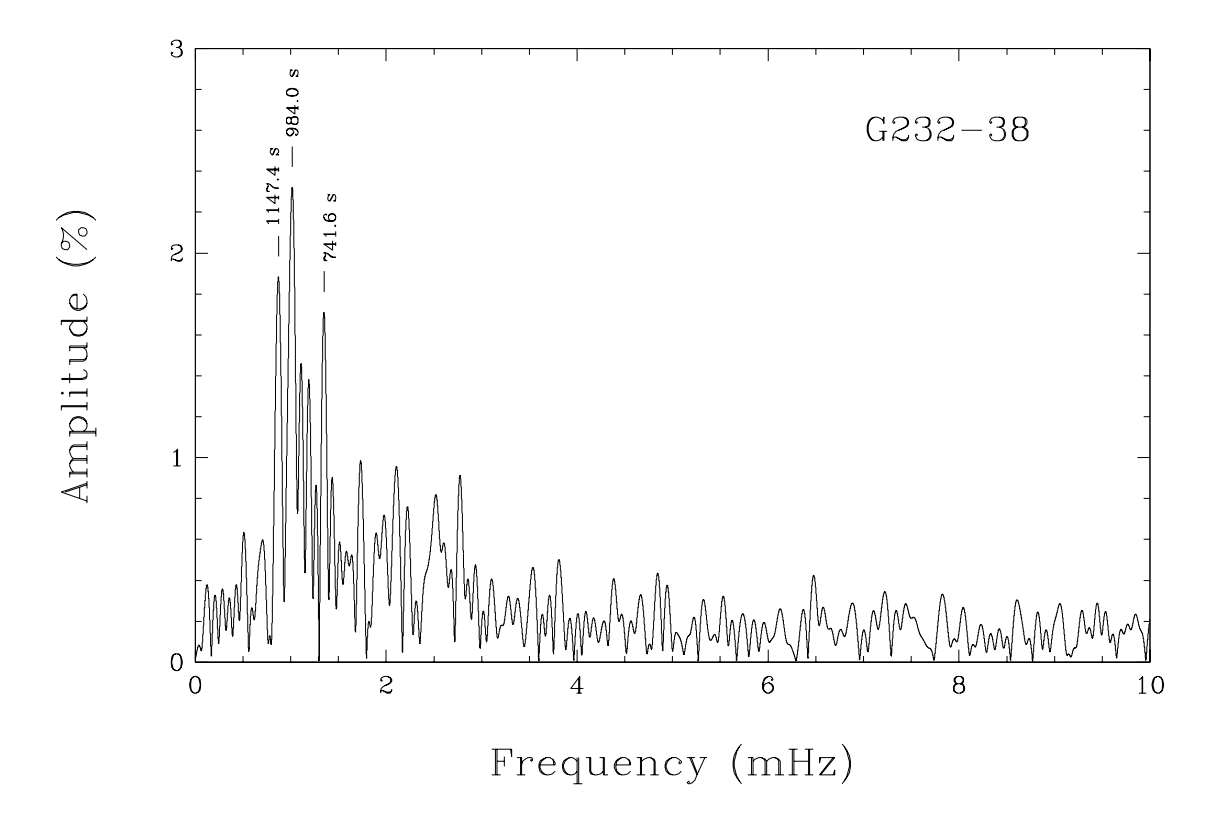
Fig. 12.— A plot of the uncertainty in  $T_{\text{eff}}$  (solid line) and  $\log g$  (dashed line) as a function of S/N for a simulated (see text) DA white dwarf with  $T_{\text{eff}} = 12,000$  K and  $\log g = 8.0$ .

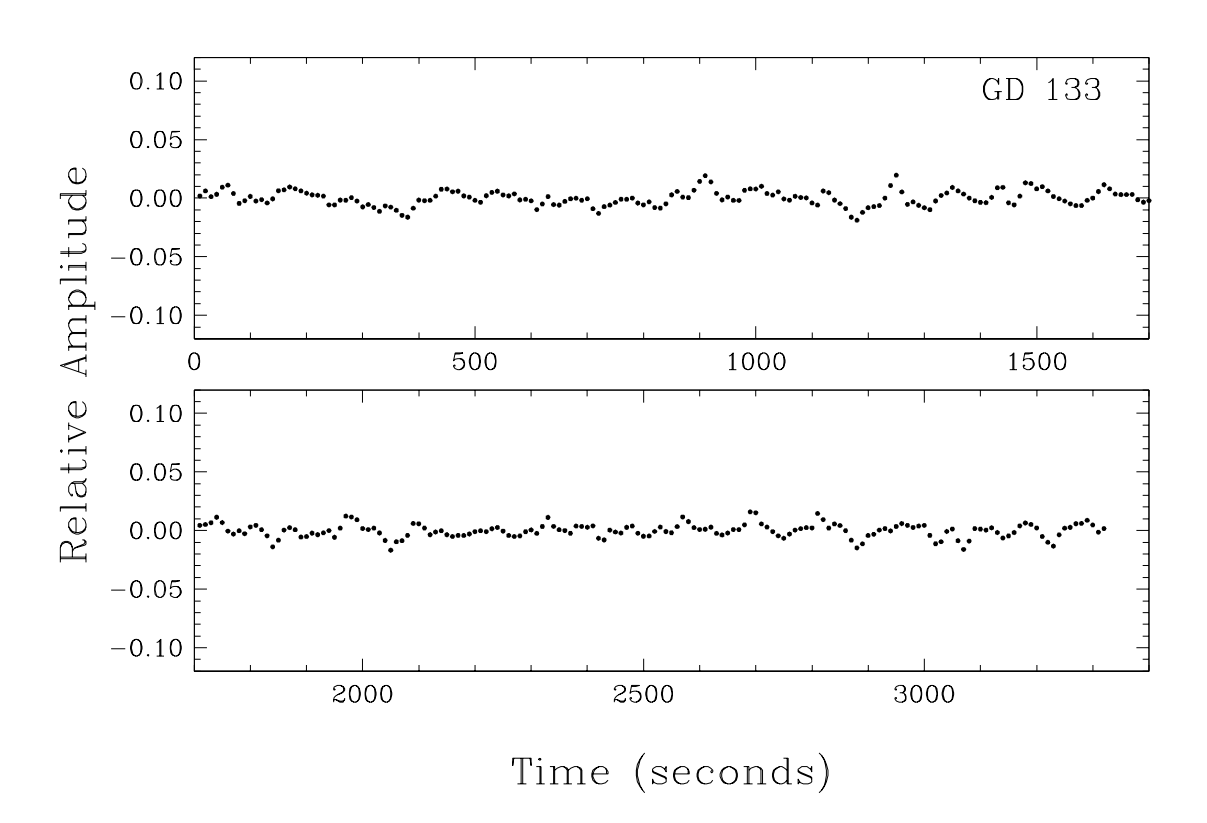
Fig. 13.— Surface gravity – effective temperature distribution for the DA stars taken from Mukadam et al. (2004a) for different S/N thresholds. The dashed lines represent the empirical blue and red edges of the instability strip defined by Bergeron et al. (2004). Open circles represent ZZ Ceti stars while the filled circles correspond to nonvariables. The open and filled triangles represent our determinations of the atmospheric parameters of WD 1338–0023 and WD 1711+6541 (*left and right symbols*, respectively) based on our own spectroscopic observations and model spectra; dashed lines join these determinations with those of Mukadam et al. (2004a).

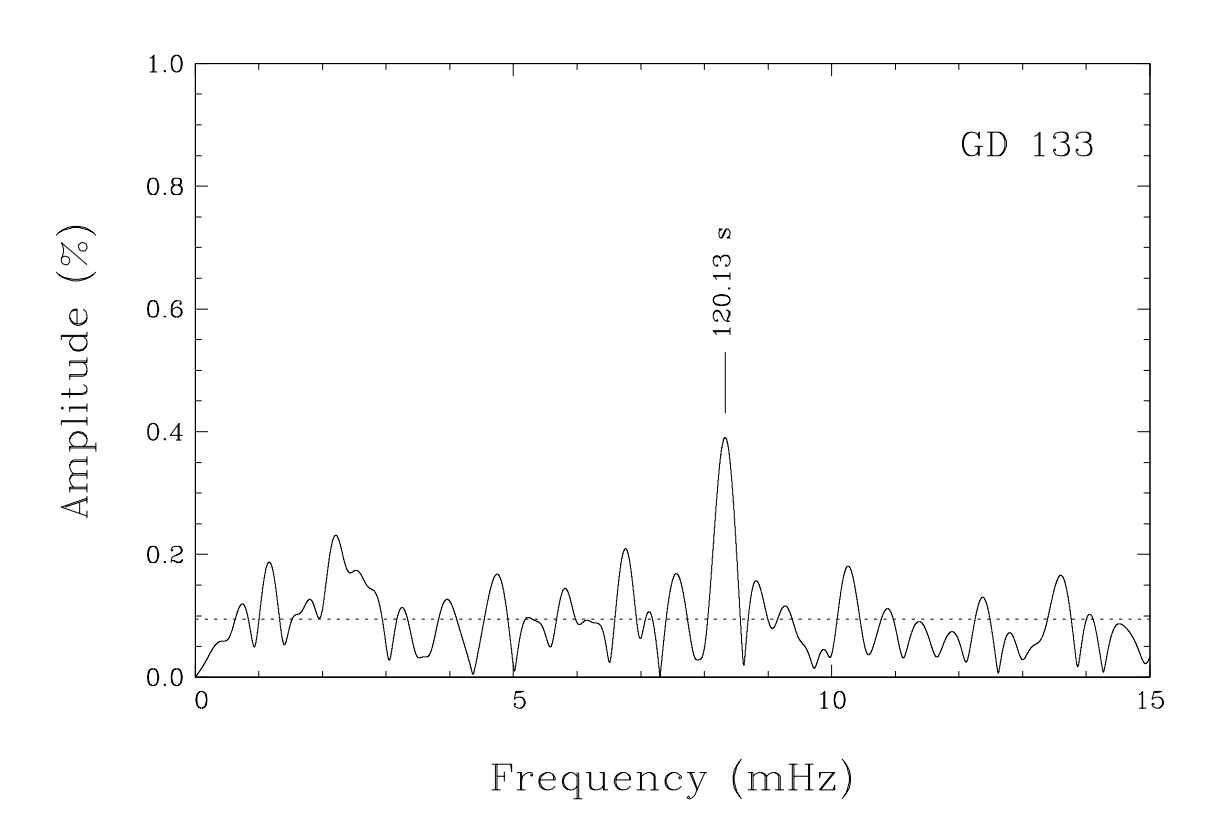
Fig. 14.— Same as Fig. 6 with the addition of all the DA white dwarfs from our ongoing spectroscopic survey of the catalog of McCook & Sion (1999). The circles correspond to objects that have been investigated for photometric variability with the open circles representing the ZZ Ceti stars, while the filled triangles correspond to objects that have not been investigated for photometric variability.

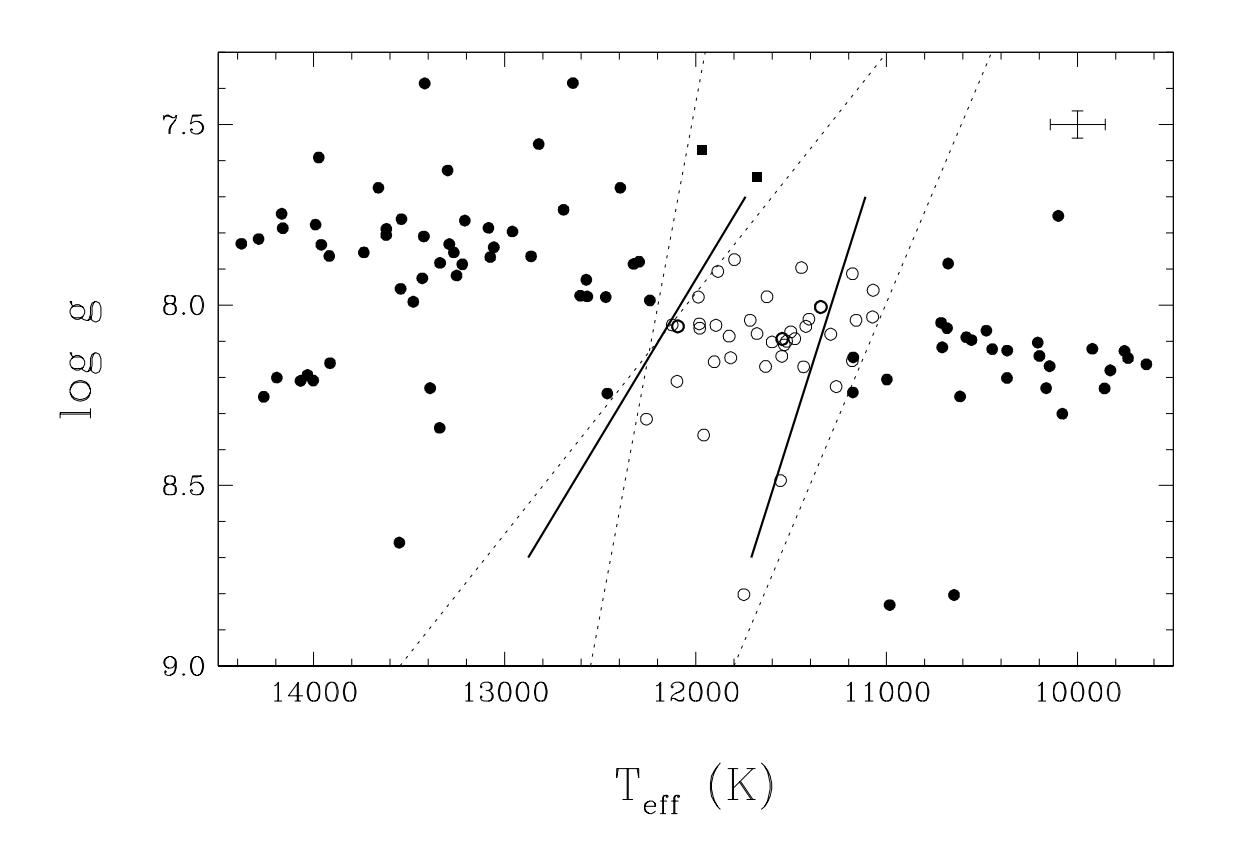


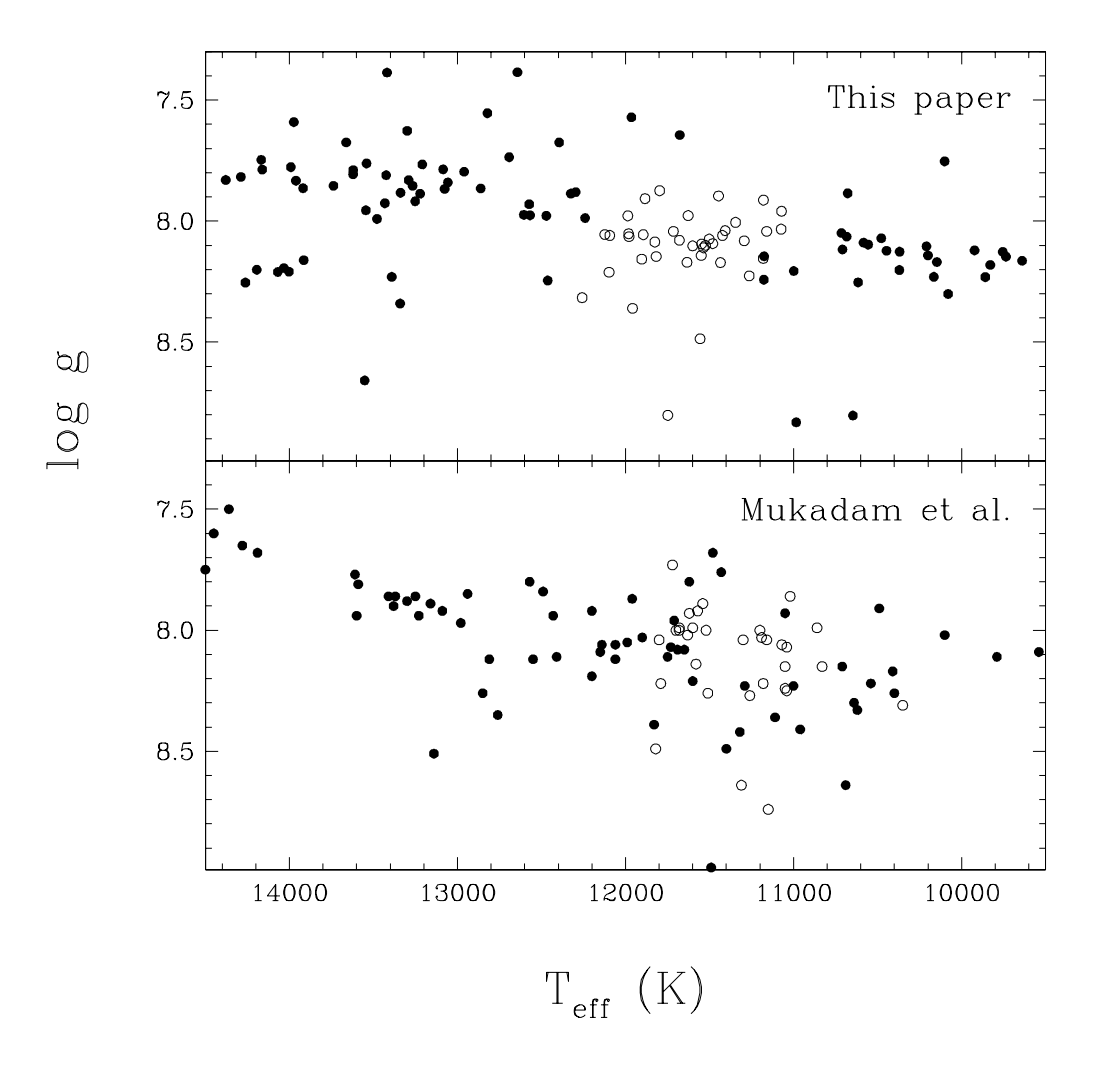


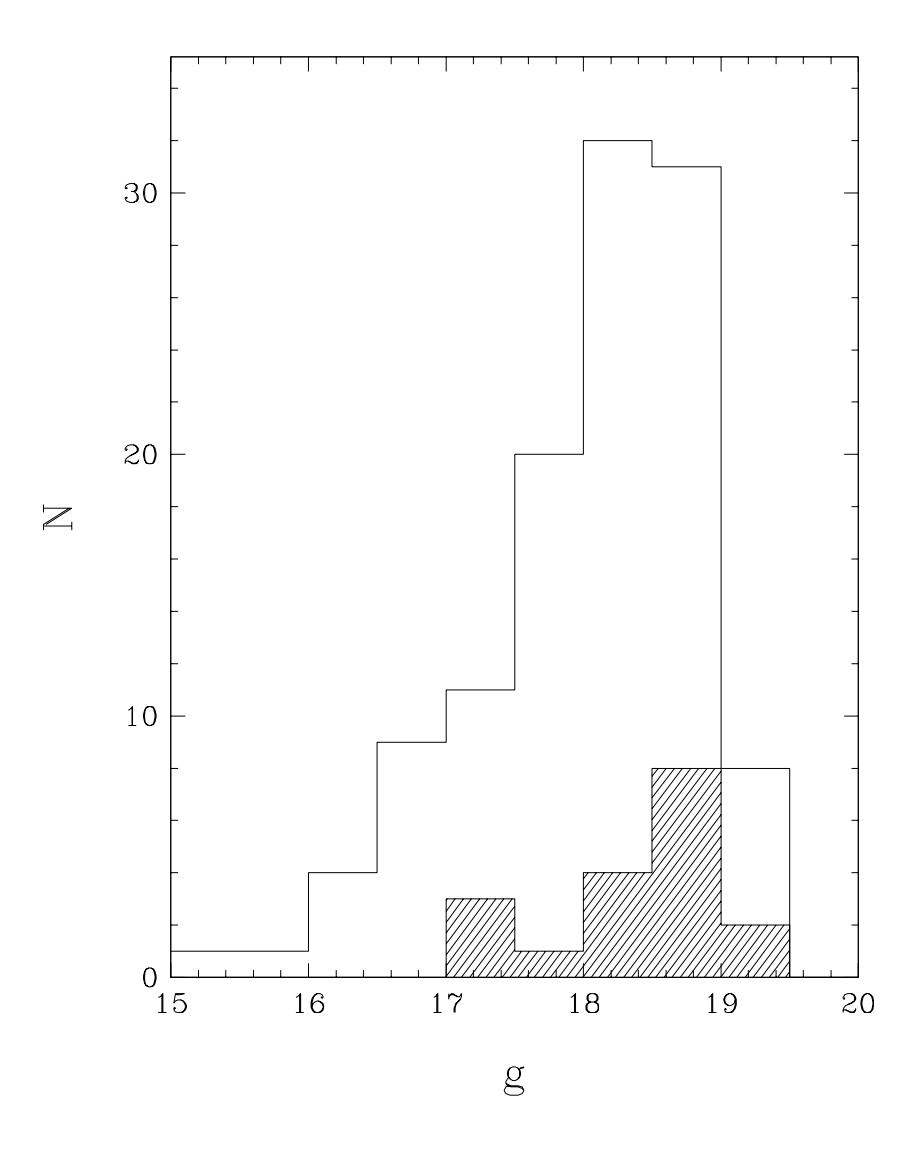


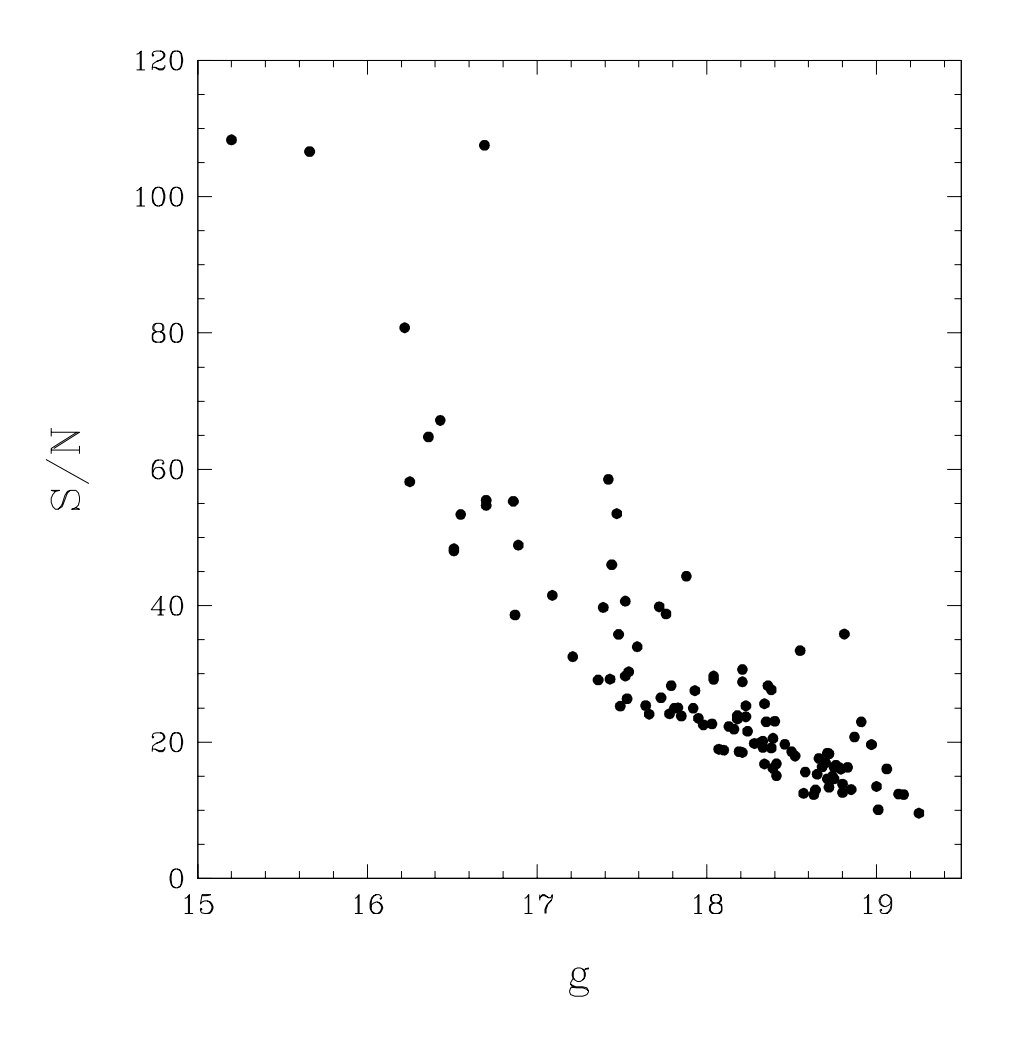












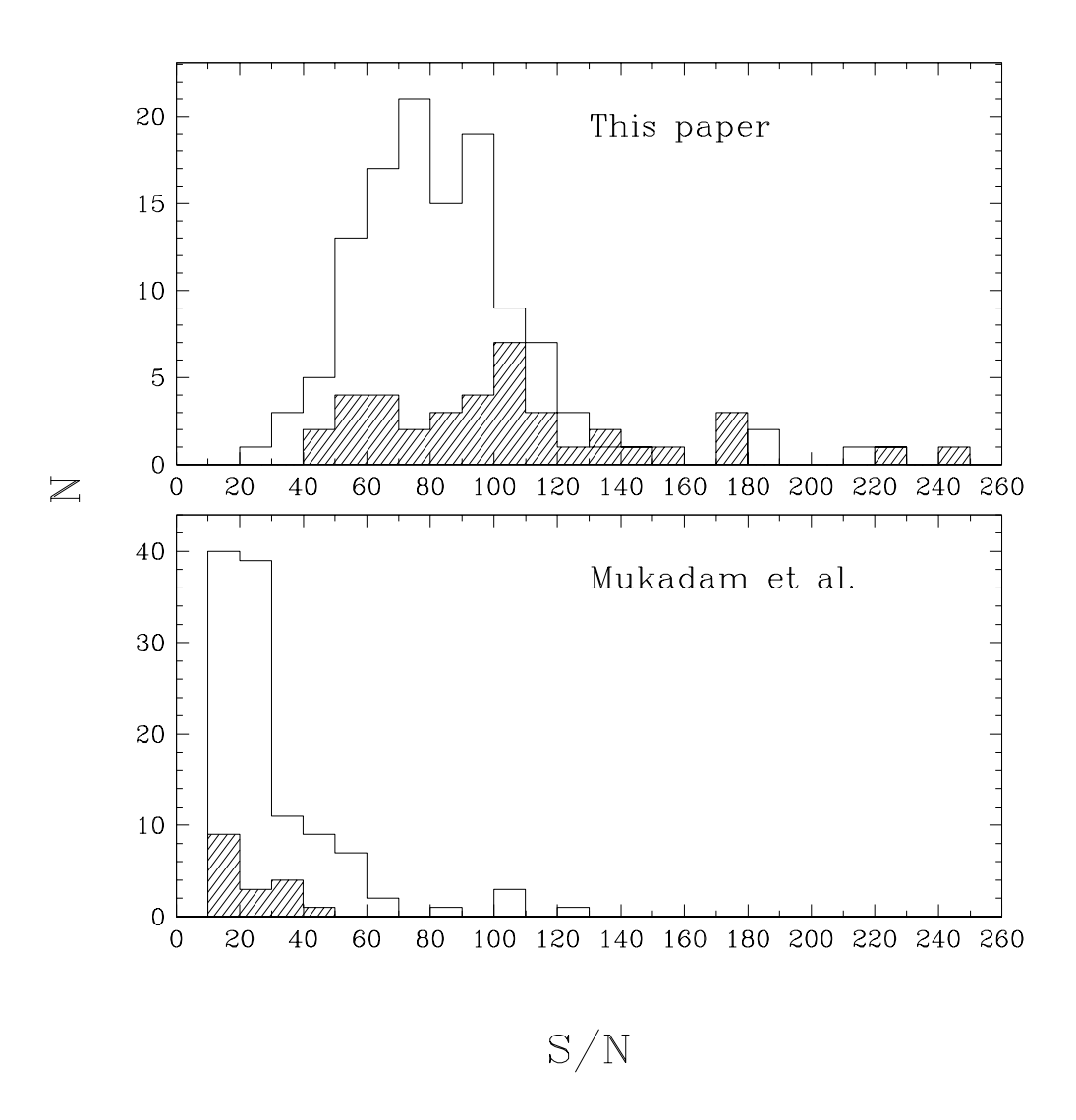


Figure 10

